Saudi Journal of Biological Sciences 30 (2023) 103820

HOSTED BY

Contents lists available at ScienceDirect

Saudi Journal of Biological Sciences

journal homepage: www.sciencedirect.com

Original article

Moringa oleifera seed based green synthesis of copper nanoparticles: Characterization, environmental remediation and antimicrobial activity

Khawla E. Alsamhary

Department of Biology, College of Science and Humanities in Al-Kharj, Prince Sattam Bin Abdulaziz University, Al-Kharj, 11942, Saudi Arabia

ARTICLE INFO

Article history:
Received 19 July 2023
Revised 11 September 2023
Accepted 21 September 2023
Available online 26 September 2023

Keywords:
Copper nanoparticle
Chromium
Dye
Remediation
Green synthesis
Antimicrobial

ABSTRACT

Textile dyes and heavy metals like hexavalent chromium [Cr(VI)] are considered major water pollutants. In addition, microbial contamination also seriously threatens potable water availability. The present study used *Moringa oleifera* seed aqueous extract to synthesize copper nanoparticles (MOS-CuNPs). MOS-CuNPs were characterized by various spectroscopy and microscopic techniques. MOS-CuNPs were shown to be effectual at removal of Cr(VI). The initial concentration of Cr(VI), contact time, pH, and temperature all impacted the removal of Cr(VI) by different concentrations of MOS-CuNPs. At low concentrations of MOS-CuNPs (0.3 mg/ml) pseudo-first order and high concentrations of MOS-CuNPs (0.4 and 0.5 mg/ml), pseudo-second order kinetics were obeyed. Thermodynamic analysis revealed that Cr(VI) was removed spontaneously, and the reaction was exothermic. In adsorption isotherm, equilibrium data followed Langmuir equation for Cr(VI) adsorption by MOS-CuNPs and maximum uptake capacity calculated was 38.6 mg/g. MOS-CuNPs efficiently removed cationic (rhodamine B, malachite green and methylene blue and) and anionic (congo red, titan yellow and methyl orange) dyes within 10 min of contact time. Further MOS-CuNPs showed antimicrobial activity against human pathogenic bacteria and fungi. Altogether, MOS-CuNPs could be used for environmental (water treatment) and biological applications.

1. Introduction

Water pollution is a major concern throughout the World, and the availability of potable water is becoming difficult. Effluents released from industries such as tannery, chrome plating, dye manufacturing, and aircraft industry contain chromium (Tumolo et al., 2020). Hexavalent chromium [Cr(VI)] is carcinogenic, mutagenic and teratogenic due to its cell-permeable nature; thereby, it produces oxidative stress and DNA damage in the cells (Zhitkovich 2011). In addition to heavy metals pollution, dyes are another major water contaminant. The degradation products of dyes are carcinogenic and pose serious health threats. Also, due to their high solubility, the presence of dye minimizes the penetration of sunlight, affecting the ecology of water systems (Al-Tohamy et al., 2022). The techniques presently available for the purification of industrial effluents have various disadvantages (high-cost equipment requirement, high energy and accumulation of toxic sludge), hence search for feasible, easily operable, cost-effective, recyclable, and highly efficient methods are required (Ahmed et al., 2022). Trivalent [Cr(III)] is considered less toxic and residues in aqueous solution. Hence, reducing Cr(VI) or removal through adsorption are considered major mechanisms for remediation (Mohan et al., 2015; Ye et al., 2021). Adsorption and mineralization of dyes are major mechanisms for dye removal from effluent. In addition to these pollutants, human pathogens in contaminated water have also been considered a serious threat. Hence, applying a method with multiple efficiencies, such as heavy metal [Cr(VI)] removal, dye degradation, and antimicrobial effect, would be advantageous.

Nanomaterials are gaining interest due to their efficiency, reusability, cost-efficiency and surface area availability for pollutants and microbes removal (Mohan et al., 2015; Tahir et al., 2022). Due to affordable, facile and environmental-friendly nature, green synthesis approach using plant extracts for surface capping and reduction of copper to produce copper nanoparticles (CuNPs) has become more popular (Din et al., 2017; Tahir et al., 2022). CuNPs have wide range of functions for use in both environmental (heavy metal and dye removal) and biological applications (anticancer, antimicrobial, increasing crop yield, anti-diabetic, anti-

Peer review under responsibility of King Saud University.

Production and hosting by Elsevier

E-mail address: k.alsamhary@psau.edu.sa

https://doi.org/10.1016/j.sjbs.2023.103820
1319-562X/

inflammatory and antioxidant) (Mohan et al., 2015; Ismail et al., 2019; Naikoo et al., 2021). CuNPs synthesized from various plant sources have shown different properties and functions. Hence, synthesizing CuNPs using new plant sources would produce NPs with different surface properties and applications.

Different parts of *Moringa oleifera* belonging to the Moringaceae family have been used as food and for medicinal purposes. In particular, *M. oleifera* seed (MOS) is gaining interest due to its functions in both environmental (bio coagulant in water purification and dye adsorption) and biological (wound healing, anti-diabetic, anti-obesity and antimicrobial) applications (Nova et al., 2020; Adesina et al., 2021; Flores et al., 2022). The presence of cationic protein and various phytochemicals (phenolics, flavonoids and tannins) in MOS has been implicated in the wide beneficial properties of MOS (Lopes et al., 2020). Due to these beneficial effects, in the present study aqueous extract of MOS was used to prepare CuNPs called MOS-CuNPs and characterized. Further, MOS-CuNPs were studied for their application in removing pollutants (Cr and dyes) and antimicrobial activity. The effectiveness of MOS-CuNPs in removing Cr(VI) was tested through batch experiments. Cr(VI) removal quantified in terms of its kinetics, adsorption isotherm, and thermodynamics. Various dyes (cationic and anionic) removal by MOS-CuNPs was studied. In addition, the antimicrobial effect of MOS-CuNPs against bacteria and fungi was investigated.

2. Materials and methods

2.1. Materials

Copper sulfate pentahydrate, potassium dichromate and diphenylcarbazide (DPC) were obtained from Sigma Aldrich, USA.

2.2. Preparation of MOS aqueous extract

M. oleifera seed (MOS) aqueous extract was prepared as previously described (Katata-Seru et al., 2018). Briefly, 10 g of MOS powder was extracted with 95% ethanol and the residue was dried. The dried residue was extracted with 100 ml of 0.1 M sodium chloride solution for 120 min at room temperature in a magnetic stirrer to obtain MOS aqueous extract.

2.3. Preparation of CuNPs using MOS aqueous extract

Copper sulfate (350 mM) solution was prepared in distilled water. To this solution, a mixture of MOS aqueous extract was added drop-wise and stirred in a magnetic stirrer at 300 rpm at 80 °C for 2 h and further for 12 h at room temperature. Formation of yellow particles confirmed the CuNPs synthesis. Centrifugation at 15,000 rpm for 20 min yielded the MOS-CuNPs. The MOS-CuNPs were washed three times with distilled water and dried at 50 °C to form a powder and stored at 4 °C for further use.

2.4. Characterization of MOS-CuNPs

The UV–visible spectrum of MOS-CuNPs was obtained using a UV–visible microplate reader (Epoch2, BioTek, USA). The morphology of the MOS-CuNPs was visualized using SEM (Jeol, USA). FT-IR analysis was done by scanning through wavelength 4000–500 cm^{-1} (Bruker, USA). The chemical property of MOS-CuNPs was examined by EDX (EDAX Inc, USA). The powder XRD analysis of dried powder of MOS-CuNPs was carried out with the scanning range between 20° and 80° (SmartLab SE, Rigaku, Japan).

2.5. Batch experiments of determining adsorption of Cr(VI) on MOS-CuNPs

DPC method employed to determine Cr(VI) concentration using a UV–visible microplate reader (Epoch2, BioTek, USA), as previously reported (Ahmed et al. 2021). The influence of initial concentration of Cr(VI) (5, 10 and 15 ppm), concentration of MOS-CuNPs (0.1, 0.2, 0.3, 0.4 and 0.5 mg/ml), pH (3, 7 and 10), temperature (20, 30 and 40 °C) and time of contact(5, 10, 20 and 30 min) on adsorption of Cr(VI) was determined.

2.5.1. Adsorption isotherm, kinetics and thermodynamics of Cr(VI) removal

Adsorption isotherm (Langmuir, Freundlich and Temkin) of MOS-CuNPs was determined as described earlier (Ayub et al., 2020; Ragadhita and Nandiyanto 2021). First-order and second-order rate equations were used to calculate the removal kinetics of Cr (VI) (Ahmed et al., 2021; Katsayal et al., 2022). The thermodynamic properties were determined as described previously (Ahmed et al., 2021; Katsayal et al., 2022). Detailed formulas and calculations are given in Supplementary. The results are given as mean ± standard deviation of experiments done in triplicate. Further regression analysis was carried out to plot the graphs.

2.6. Catalytic reduction or adsorption of dyes by MOS-CuNPs

The reduction or adsorption of various dyes such as congo red (CGR), methyl orange (MO), methylene blue (MB), malachite green (MG), rhodamine B (RHB) and titan yellow (TY) were studied. In a cuvette, 1 mg of MOS-CuNPs was added to 0.03 mM dye solution (1.5 ml). The reaction was carried out in the presence or absence of 0.25 ml of sodium borohydride (NBH; 0.2 M). The variation in the absorbance was monitored by scanning from 200 to 800 nm using a UV–visible microplate reader (Ismail et al., 2019).

2.7. Determination of the antimicrobial activity of MOS-CuNPs using zone of inhibition studies

Agar well diffusion method was employed to determine antimicrobial activity of MOS-CuNPs. The organisms used were Gram-negative (*Escherichia coli* and *Klebsiella pneumonia*), Gram-positive (*Enterococcus faecalis* and *Staphylococcus aureus*) and fungi (*Candida albicans*). Mueller-Hinton agar (MHA) and sabouraud dextrose agar (SDA) media were used for bacterial and fungal culture. Inoculum containing 10^6 cfu/mL of the freshly prepared microbial culture was spread onto the agar plate. Then, three wells (8 mm in diameter) were punched into the agar medium. Two wells in each plate contain 25 μg/ml and 100 μg/ml of MOS-CuNPs. For gram-positive and gram-negative bacteria cultures, 10 μg/ml of gentamicin and 30 μg/ml of chloramphenicol were used as the positive control. For fungal culture, 25 μg/ml of fluconazole was used as a positive control.

3. Results

3.1. Characterization of MOS-CuNPs

The UV–visible spectrum of MOS-CuNPs is shown in Fig. 1A. MOS-CuNPs showed λ_{max} at 662 nm. SEM image revealed the amorphous nature of the MOS-CuNPs (Fig. 1B). Cu in MOS-CuNPs was detected using EDX (Fig. 1C). Other than Cu, the distribution of O and Cl was also observed. XRD spectra of MOS-CuNPs showed diffraction peaks for CuO (monoclinic) at 32.18 (110), 36.19 (111), 39.63(202), 49.87(020), 53.41(113), 61.28 (311) and 73.5° (004) (Fig. 1D). Uniform-sized MOS-CuNPs were formed with an average

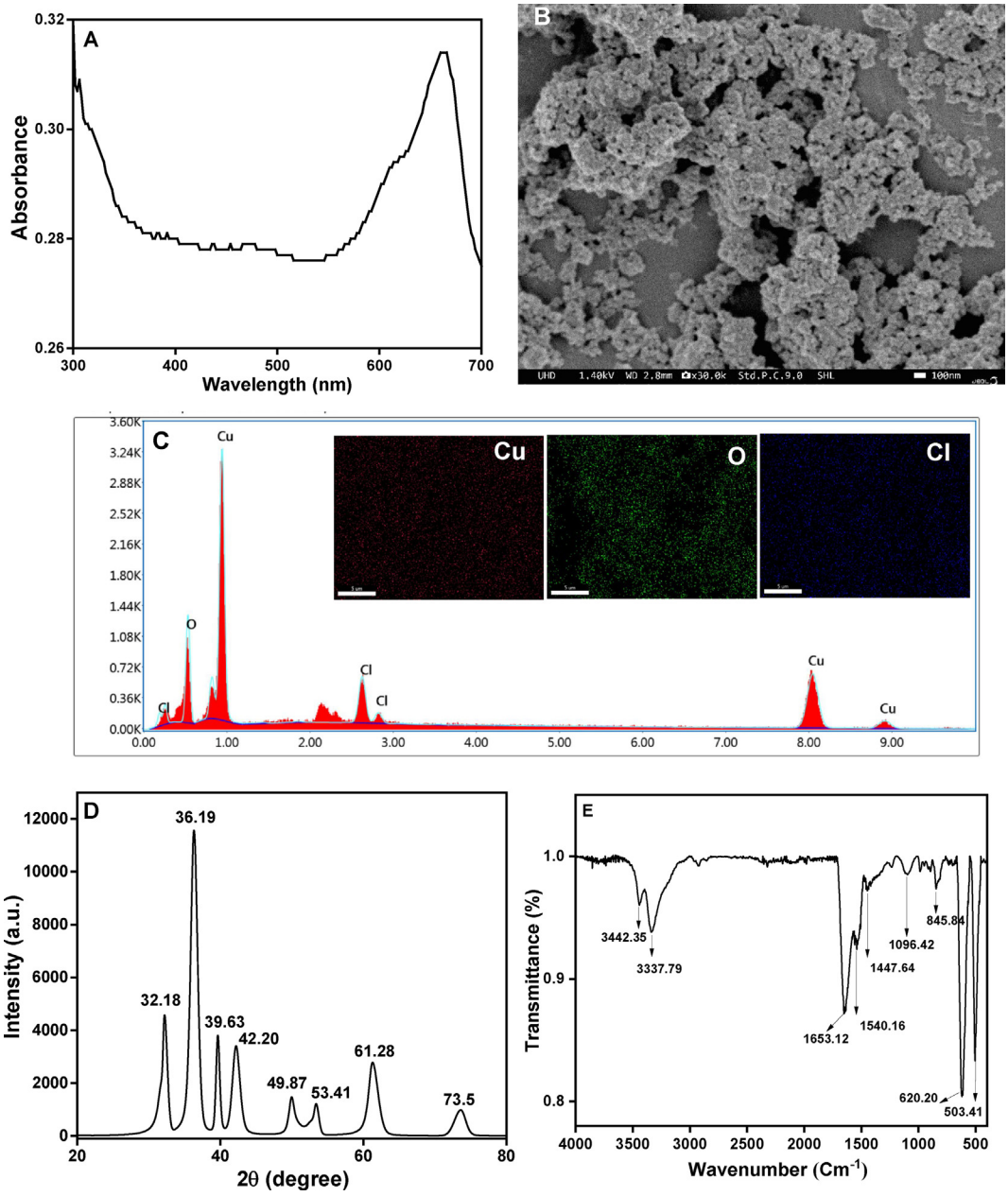

Fig. 1. Characterization of MOS-CuNPs. (A)UV–visible spectrum, (B) SEM image, (C) EDX (inset: elemental distribution of metal on the surface), (D)XRD spectrum, (E) FTIR spectrum.

dimension of 7.38 nm as calculated by Debye-Scherrer formula. The FT-IR spectra of MOS-CuNPs showed peaks at 3442.35, 3337.79, 1653.12, 1540.16, 1447.64, 1096.42 and 845.84, which corresponds to OH of alcohol/phenol, NH of primary and secondary amine, C═C of imines, N═O of nitro, CH of alkane, C—O stretch and C—Cl bond, respectively. Further peaks at 620.21 and 503.41 correspond to the CuO bond (Fig. 1E).

3.2. Removal of Cr(VI) by MOS-CuNPs

Different MOS-CuNP concentrations were shown to remove Cr (VI) dose-dependently (Fig. 2). The MOS-CuNPs could efficiently remove the Cr(VI) at all the initial concentrations of 5 ppm, 10 ppm and 15 ppm. Further parameters were evaluated in the presence of a 10 ppm Cr(VI) because the Cr(VI) elimination was marginally reduced at a 15 ppm Cr(VI). The Cr(VI) removal by MOS-CuNPs at various pH is shown in Fig. 3. At acidic pH, 0.1 mg/ml (lowest concentration) of MOS-CuNPs removed ≈70% of Cr(VI). However, at pH 7 and 10, the percentage removal was affected by the lowest concentration of MOS-CuNPs. Only high concentrations of MOS-CuNPs (0.3–0.5 mg/ml) could efficiently remove the Cr(VI) at pH 7 and 9. At the concentrations from 0.1 to 0.3 mg/ml of MOS-CuNPs, Cr(VI) was removed time-dependently (Fig. 4). In the presence of 0.4 mg/ml and 0.5 mg/ml of MOS-CuNPs, the removal of Cr(VI) reached ≈ 60% and ≈ 80% within 5 min of contact time between Cr(VI) and MOS-CuNPs.

The first-order and second-order kinetic plots of the MOS-CuNPs ability to remove Cr(VI) are depicted in Fig. 5A and B, respectively. In the presence of 0.3 mg/ml of MOS-CuNPs, the correlation coefficient determined that the reaction followed pseudo-first-order kinetics (Table 1). However, in the presence of an increased concentration of MOS-CuNPs, the correlation coefficient

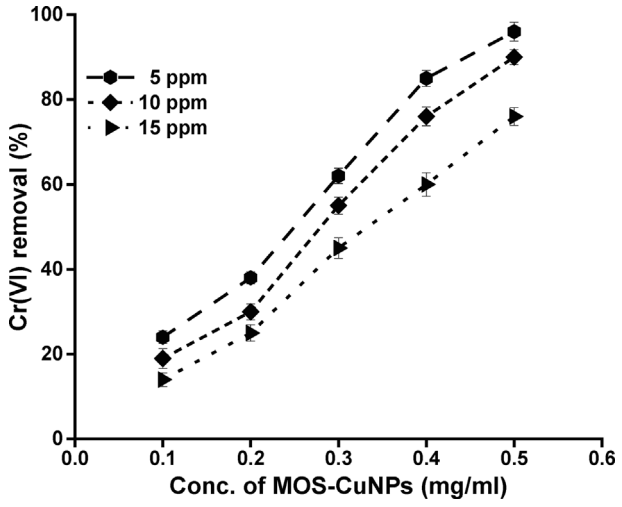

Fig. 2. Chromium initial concentration influence on Cr(VI) removal by various MOS-CuNPs concentrations. (Initial concentration of Cr(VI) = 5 ppm, 10 ppm and 15 ppm; Temperature = 30 °C; time = 30 min, pH = 7.0). n = 3.

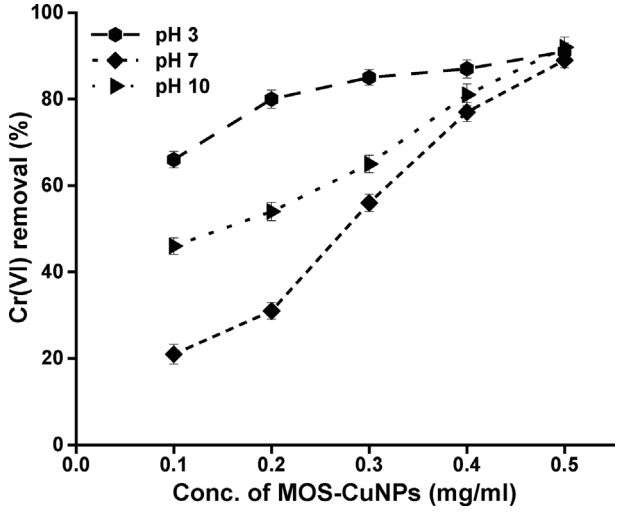

Fig. 3. Ph influence on cr(vi) removal by various concentrations of mos-cunps. (Initial concentration of Cr(VI) = 10 ppm; Temperature = 30 °C; time = 30 min; pH = 3.0, 7.0 and 10.0). n = 3.

obtained indicated that pseudo-second-order kinetics was followed. The effect of different temperatures on Cr(VI) (10 ppm) removal by various concentrations of MOS-CuNPs at pH 7 is given in Fig. 6. A dose-dependent effect was observed in various concentrations of MOS-CuNPs at different temperatures. Only marginal impact on metal ion removal was found at various temperatures when MOS-CuNPs were present in high concentrations (0.5 mg/ml). The Van't Hoff plot is given in Fig. 7, and thermodynamics parameters are given in Table 2. The ΔG^0 value was positive at 20 °C in the presence of 0.3 and 0.4 mg/ml of MOS-CuNPs. However, with increased temperature, ΔG^0 value was negative at these concentrations. In the presence of 0.5 mg/ml of MOS-CuNPs, ΔG^0 value was negative from low to high temperature.(See Table 3)

Langmuir (Fig. 8A), Freundlich (Fig. 8B) and Temkin (Fig. 8C) assessment of metal ion removal is determined. In comparison to Freundlich model, Langmuir model fitted well with a coefficient of regression value, 0.999. The values of the separation factor (R_L) are less than 1, and the 1/n value in the Freundlich model was less than 1. The coefficient of regression value for the Temkin model was 0.997.

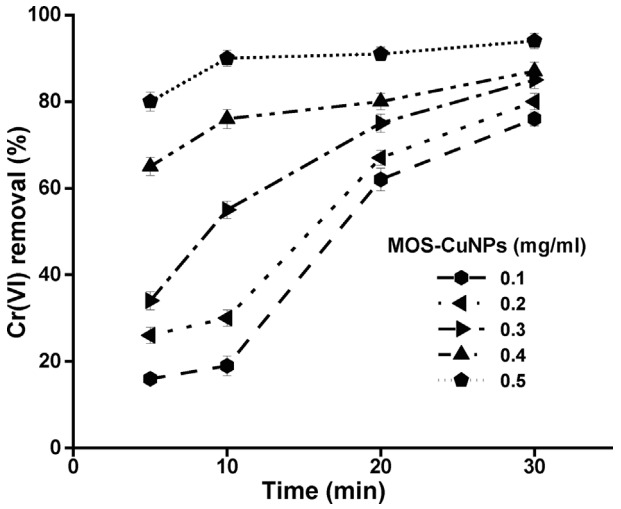

Fig. 4. Time effect on Cr(VI) removal by various concentrations of MOS-CuNPs. (Initial concentration of Cr(VI) = 10 ppm; pH = 7.0; Temperature = 30 °C; time = 5, 10, 20 and 30 min). n = 3.

3.3. Removal of various dyes by MOS-CuNPs

The removal of various dyes by MOS-CuNPs in the presence and absence of NBH has been monitored by scanning from 200 nm to 700 nm using a UV–visible spectrophotometer (Fig. 9). The decay in the respective absorption bands for various dyes, CGR (Fig. 9A), MO (Fig. 9B), MB (Fig. 9C), MG (Fig. 9D), RHB (Fig. 9E) and TY (Fig. 9F), have been observed within 5 min of contact time with the MOS-CuNPs. MOS-CuNPs alone could remove the dyes CGR, MO, MB, MG and TY. In the case of RHB, the presence of reducing agent (NBH) and a catalyst (MOS-CuNPs) was found to be required for the dye removal.

3.4. Antimicrobial activity of MOS-CuNPs

MOS-CuNPs showed an antibacterial effect against the human pathogenic bacteria, *S. aureus* and *K. pneumonia,* at a lower concentration of 25 μg/ml (Table 4). On the other hand, MOS-CuNPs showed a zone of inhibition against *E. faecalis*, *E. coli* and *C. albicans* at a higher concentration of 100 μg/ml.

4. Discussion

The peak position and spectral shape of any NPs synthesized using plant extracts in UV–visible spectrum are sensitive to reducing agents and stabilizers in the extract, size of the metal and dielectric constant. In concordance to MOS-CuNPs (662 nm), various studies found that the absorbance band of CuNPs were 550 nm to 700 nm (Mohan et al., 2015; Khani et al., 2018; Ismail et al., 2019). MOS aqueous extract was previously found to contain polysaccharides, water-soluble cationic proteins and secondary metabolites (phenolics and flavonoids) (Adebayo et al., 2018; Nouhi et al., 2019). All these components in MOS could have contributed to the reduction of Cu into Cu_2ONPs, and further annealing resulted in crystalline cupric oxide NPs (CuONPs). The aggregation of the NPs might be due to the surface coating of different plant metabolites. Such aggregation of CuNPs was observed in previous studies wherein CuNPs were synthesized using orange peel extract or jujube fruit extract (Khani et al., 2018; Mahmoud et al., 2021). The EDX showed the homogenous distribution of Cu on the surface of the MOS-CuNPs formed. Other than Cu, the distribution of O and Cl, which were present in the MOS aqueous extract, have been

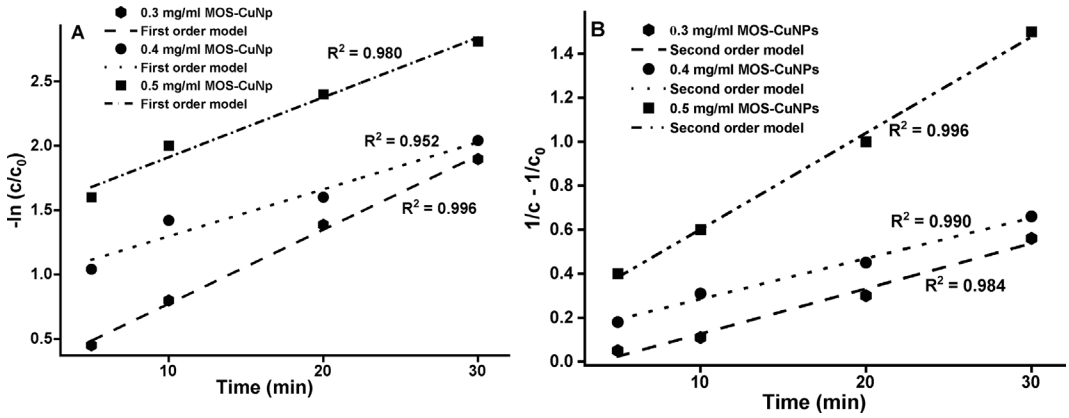

Fig. 5. Cr(VI) removal kinetics. Plot using the first-order kinetic equation (A) and second-order kinetic equation (B). n = 3.

Table 1
Kinetic parameter for Cr(VI) removal by different concentrations of MOS-CuNPs at various time (pH: 7; temperature: 40 °C). n = 3.

Kinetic model	MOS-CuNPs (mg/ml)		
	0.3	0.4	0.5
Pseudo-first order			
K_1 (min^{-1})	0.057	0.036	0.046
Correlation (R^2)	0.996	0.952	0.980
$T_{1/2}$ (min)	12.15	19.25	15.06
Pseudo-second order			
K_2 (mg/ml/min)	0.020	0.018	0.043
Correlation (R^2)	0.984	0.990	0.996
$T_{1/2}$ (min)	34.65	38.5	16.11

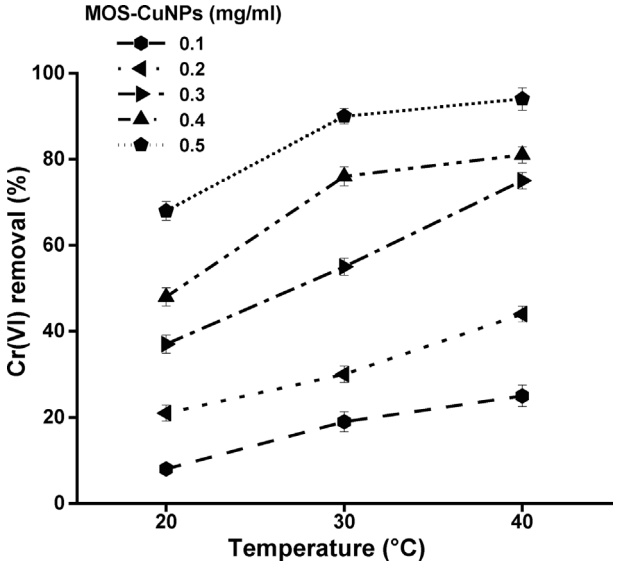

Fig. 6. Temperature effect on Cr(VI) removal by various concentrations of MOS-CuNPs. (Initial concentration of Cr(VI) = 10 ppm; Temperature = 3 °C, 37 °C, 45 °C, 60 °C and 80 °C; time = 30 min; pH = 7.0). n = 3.

observed. The peaks obtained in XRD are in agreement with previous reports. In particular, peaks between 35 and 39° indicate the crystalline nature of MOS-CuNPs (Amin et al., 2021; Alhalili 2022). FTIR analysis of MOS-CuNPs showed the presence of functional groups from various secondary metabolites that might be present in the MOS aqueous extract due to the capping of metabolites in the extract. The peak observed in 620.21 and 503.41 corresponds to Cu—O along the direction due to monoclinic crystalline CuNPs (Singh et al., 2016; Elango et al., 2018).

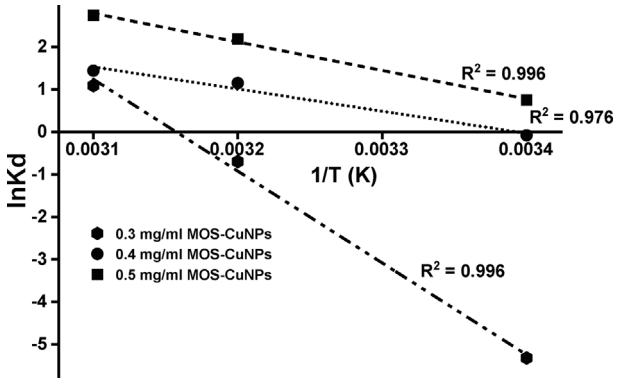

Fig. 7. Thermodynamics of Cr(VI) removal. Natural logarithm of the equilibrium constant of Cr(VI) removal vs the reciprocal of the reaction temperature in K. n = 3.

Adsorption and reduction (owing to internal electron transfer) are the processes involved in Cr(VI) removal by metal NPs, including CuNPs (Ahmed et al., 2021; Ye et al., 2021). The removal of Cr (VI) in water is enhanced because zerovalent Cu is known to donate electrons in the aqueous media (Rivero-Huguet and Marshall 2009; Ye et al., 2021). The surface area and atom efficiency (metal atom fraction available for reaction) are higher in nanoscale MOS-CuNPs. Such properties would have also contributed to Cr(VI) removal (Rivero-Huguet and Marshall 2009). Cr (VI) exists as oxyanions ($HCrO_4^-$, $Cr_2O_7^{2-}$ and CrO_4^{2-}) in aqueous solution at low pH (acidic condition). As well as, under such conditions, the NPs become protonated on the surface. Hence attraction between protonated MOS-CuNPs and Cr oxyanions would have led to the uptake of Cr (Al-Sou'od 2012; Mohan et al., 2015). The pH 6.8 has been found to be a zero-point charge for CuO NPs; hence, as the pH increases, the MOS-CuNPs' surface would have attained a negative charge (Goswami et al., 2012). At such conditions, the repulsive force would have hindered the adsorption of Cr oxyanion species on MOS-CuNPs. Also, at alkaline pH, the OH^- ions in the solution would have competed with the Cr oxyanions for the surface available on the MOS-CuNPs (Ye et al., 2021). However, as the concentration of MOS-CuNPs increased, the reaction medium pH did not affect the Cr(VI) elimination, which could be attributed to increased adsorption site availability. In prior work, Cr(VI) adsorption on spherical bismuth bromide oxide was observed at alkaline pH via anion exchange (Jia et al., 2019). A similar phenomenon could have involved the adsorption of Cr oxyanion species on MOS-CuNPs. The Cr(VI) removal by MOS-CuNPs was instantaneous and reached saturation in 20 min, which might be due to the availability of more adsorption sites at the initial stage,

Table 2
Thermodynamic parameters for Cr(VI) removal by different concentrations of MOS-CuNPs at various temperature (pH: 7; time: 30 min). n = 3.

MOS-CuNPs (mg/ml)	Temperature (K)	ΔG^0 (J/mol)	ΔS^0 (J/K/mol)	ΔH^0 (J/mol)
0.3	293	12959.5	68.24	−21611.71
	303	−498.79		
	313	−2836.48		
0.4	293	194.88	17.71	−5221.42
	303	−2897.01		
	313	−3741.28		
0.5	293	−1834.30	23.56	−6703.57
	303	−5516.92		
	313	−7130.25		

Table 3
Isotherm parameters for Cr(VI) removal by MOS-CuNPs [Cr(VI): 10 ppm; MOS-CuNPs: 0.3 mg/ml; pH: 7; contact time: 30 min] n = 3.

Type of isotherm	Parameters	MOS-CuNPs
Langmuir	q_{max} (mg/g)	38.46
	K_L (L/mg)	0.234
	R_L	0.078
	R^2	0.999
Freundlich	K_f	8.47
	1/n	0.482
	R^2	0.977
Temkin	B_T (J/mol)	7.36
	K_T	2.67
	R^2	0.997

which has been saturated as time progressed due to occupancy of the sites by Cr(VI) oxyanions.

In the presence of low concentrations of MOS-CuNPS, a pseudo-first-order reaction was followed. It is assumed that physisorption limited the Cr(VI) adsorption rate onto the MOS-CuNPS. The regression line not passing the origin depicts physical adsorption or interaction between the adsorbent and metal ion has impacted the Cr(VI) removal (Geng et al., 2009). However, at higher concentration of MOS-CuNPs chemisorption (pseudo-second order reaction) has influenced the removal (Mohan et al., 2015). Also, the concentration of one of the reactants, that is MOS-CuNPs might be far greater than Cr(VI) in the solution, hence removal of Cr(VI) has predominantly followed pseudo-second order kinetics (Mohan et al., 2015; Ye et al., 2021, Katsayal et al., 2022).

Temperature has influenced the removal of the Cr(VI) by MOS-CuNPs. The ΔS^0 value was positive, and ΔH^0 value was negative. This shows the feasibility and spontaneity of Cr(VI) removal in various concentrations of MOS-CuNPs at different temperatures. The exothermic nature and randomness in the reaction have been indicated by negative enthalpy (ΔH^0) and positive entropy (ΔS^0), respectively. The results are in correlation with the previous study, in which CuNPs prepared using the hydrothermal method showed exothermic nature of the Cr(VI) removal (Noli et al., 2023), in contrast to other studies that showed endothermic reaction (Mohan et al., 2015, Ye et al., 2021). For effective adsorption, denuding of Cr(VI) hydration sheath when present in aqueous solution is necessary for adsorption on the MOS-CuNPs. Hence, one possible explanation of the exothermicity of the enthalpy in the case of MOS-

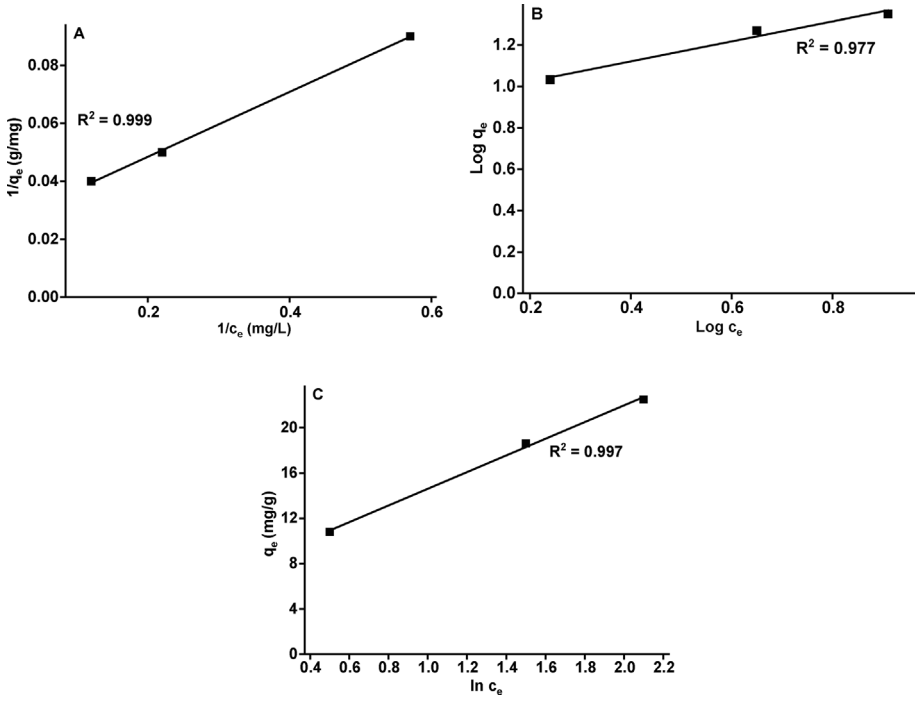

Fig. 8. Adsorption isotherm. Langmuir(A), Freundlich (B) and Temkin (C) adsorption isotherm plots for Cr(VI) removal by MOS-CuNPs.(Initial concentration of Cr (VI) = 5 ppm, 10 ppm and 15 ppm; MOS-CuNPs = 0.3 mg/ml; Temperature = 30 °C; time = 30 min, pH = 7.0). n = 3.

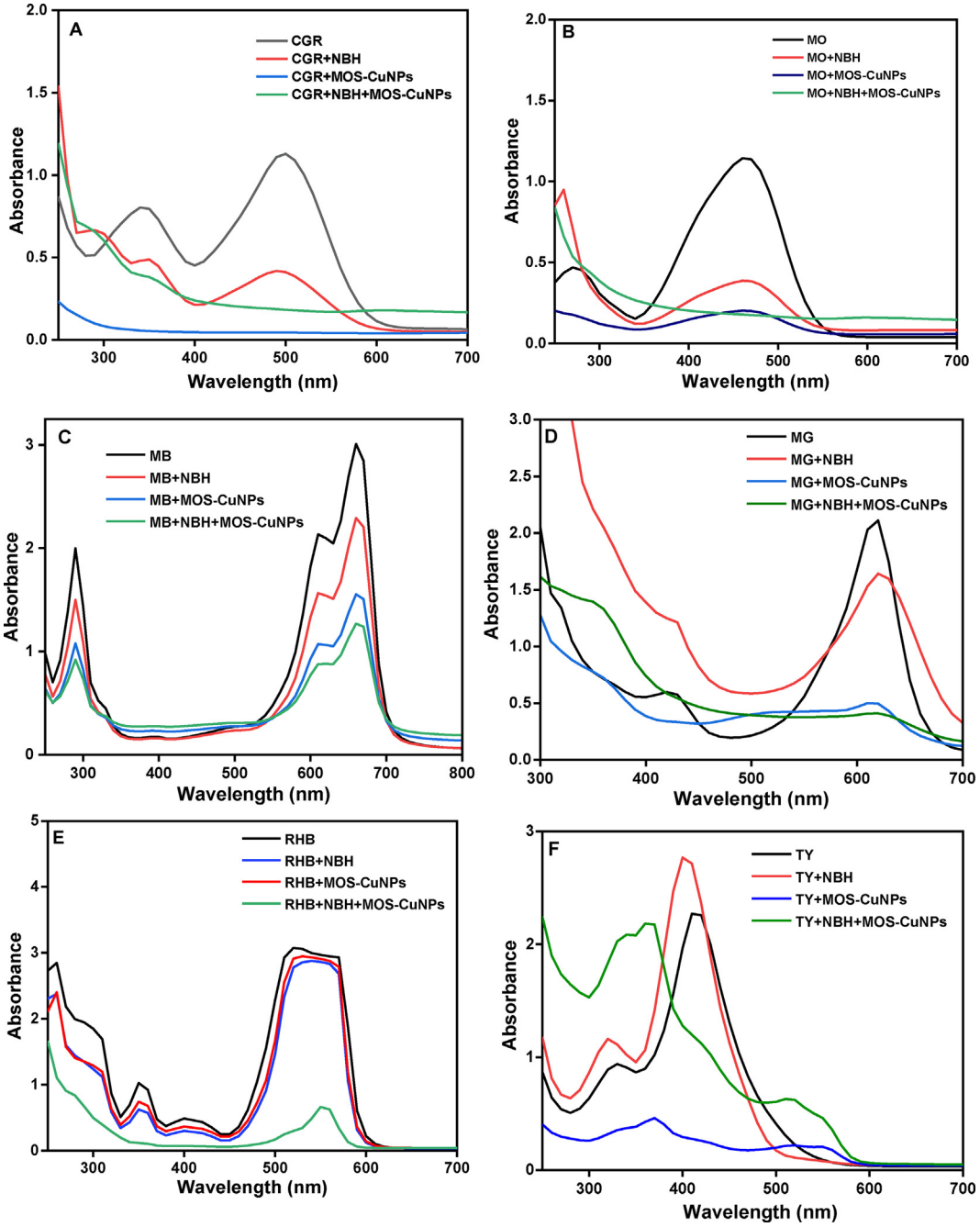

Fig. 9. Dye removal by MOS-CuNPs. Changes in adsorption spectra of various dyes, congo red (CGR; A), methyl orange (MO; B), methylene blue (MB; C), malachite green (MG; D), rhodamine B (RHB; E) and titan yellow (TY; F) by treatment with MOS-CuNPs.

Table 4
Antimicrobial activity (zone of inhibition in mm) by MOS-CuNPs against human pathogens. n = 3.

Organisms	Zone of inhibition (mm)		
	Control antibiotic	MOS-CuNPs (µg/ml)	
		25	100
Staphylococcus aureus	23 ± 0.5	10 ± 1.1	13 ± 0.9
Enterococcus faecalis	14 ± 1.2	–	13 ± 0.8
Escherichia coli	20 ± 1.3	–	15 ± 0.7
Klebsiella pneumonia	20 ± 0.9	12 ± 1.2	14 ± 0.9
Candida albicans	33 ± 1.2	–	15 ± 1.1

CuNPs might be excess energy required for Cr(VI) attaching to the surface in comparison to energy required for the dehydration process of Cr(VI) (which is an endothermic reaction) in aqueous solution (Al-Sou'od 2012).

The fitness of Langmuir isotherm demonstrates monolayer adsorption and uniform adsorption energy distribution over the surface of MOS-CuNPs. The R_L value favours the adsorption phenomenon, and a strong affinity exists between Cr(VI) and MOS-CuNPs (Mohan et al., 2015; Alhalili 2022). By the Temkin model, it has been understood that the adsorption binding energy is uniformly distributed on the surface of MOS-CuNPs (Ragadhita and Nandiyanto 2021). The results of isotherm models correlate with the kinetic model wherein the presence of 0.3 mg/ml of MOS-CuNPs in the reaction followed first-order kinetics, which means

physisorption is favoured. Altogether, removing Cr(VI) by MOS-CuNPs was efficient and in line with the previous reports (Rivero-Huguet and Marshall 2009; Mohan et al., 2015; Ye et al., 2021).

MOS-CuNPs could remove cationic (MB, MG and RHB) and anionic dyes (CGR, MO and TY) within 10 min of contact time. In the UV–visible spectrum of all the dyes studied, the blue or red shift of the absorbance band has not been found in the presence of MOS-CuNPs; rather, a decrease in the absorption band has been witnessed. These findings suggest that MOS-CuNPs might have decomposed and mineralized the dye molecules studied. However, the phenomenon of adsorption of the dyes on the MOS-CuNPs surface similar to that of metal ions cannot be ignored. Previous studies have shown that dye as an electron acceptor, and NBH as an electron donor might adsorb onto the nanocatalyst (MOS-CuNPs) surface through electrostatic interaction. (Mohammadi et al., 2020). On the surface of the catalyst, the electron transfer takes place without any hindrance or kinetic barrier due to which reduction/decolourization of the dye might take place. The formed product might be desorbed from the MOS-CuNPs surface, diffused to the solution, or further mineralized (Ghaffar et al., 2021; Rafique et al., 2022). From previous studies, various chemical reactions such as breakage of azo-bond, deamination and deethylation were found to be associated with CuNPs-mediated dyes degradation (Ghaffar et al., 2021; Rafique et al., 2022). Similar mechanisms might have been involved in the case of MOS-CuNPs to remove various dyes in the present study.

CuNPs are known for antimicrobial activity (Singaravelu et al., 2022; Al-Enazi et al., 2023). In a previous study, it was observed through SEM that cavities/pits in the bacterial cell wall were formed due to CuNPs interaction with *E. coli* (Raffi et al., 2010). Due to nano size, MOS-CuNPs would have provided a larger surface-to-volume ratio for the adhesion of NPs on the bacteria due to opposite electrical charges (Raffi et al., 2010; Tahir et al., 2022). Inside the cells, CuNPs have altered the functions of proteins and enzymes (Wang et al., 2017). In addition, releasing metal ions inside the microbial cells would increase oxidative stress, thereby killing the microbes (Gurunathan et al., 2012). NPs were found to affect the bacteria indirectly outside the bacterial cell by altering the surrounding charge environment (Tahir et al., 2022). CuNPs are known for antifungal activity inhibiting ergosterol production (Ma et al., 2022). Also, the morphogenesis of *C. albicans* is disturbed due to altered gene expression involved in yeast-to-hyphae switching by CuNPs (Padmavathi et al., 2020). Due to the antifungal activity of MOS-CuNPs, it could be used in dentistry applications.

CuNPs prepared using various other sources have shown the difference in efficiency for removal of Cr(VI) or dyes (Rivero-Huguet and Marshall 2009; Mohan et al., 2015; Ismail et al., 2019; Ye et al., 2021; Rafique et al., 2022). The advantage of MOS-CuNPs is they showed Cr(VI) and dye removal within a short contact time between adsorbent and adsorbate. Also, the degradation of most of the dyes studied by MOS-CuNPs was spontaneous and did not required a reducing agent. MOS contains cationic protein due to which it is used as flocculation/coagulation agent (Nouhi et al., 2019). MOS has been reported as a biosorbent for chromium and dye removal (Ghebremichael et al., 2010; Khamis Soliman et al., 2019; Adesina et al., 2021). Hence surface decoration or capping of the MOS active constituents on MOS-CuNPs would have also played an important role in efficiently removing Cr(VI) and dye. In addition, the antimicrobial property shown by MOS-CuNPs would be further advantageous in water treatment and biological applications.

5. Conclusion

MOS-CuNPs were synthesized using an aqueous extract of MOS and characterized. MOS-CuNPs efficiently removed Cr(VI) which was influenced by the pH of the solution. The kinetic model demonstrated pseudo-first order and pseudo-second order reactions in the presence of low concentration (0.3 mg/ml) and high concentrations (0.4–0.5 mg/ml) of MOS-CuNPs, respectively, for Cr(VI) removal. The equilibrium data for Cr(VI) adsorption followed Langmuir equation and maximum uptake capacity calculated was 38.6 mg/g. Thermodynamics studies described the spontaneous removal of Cr(VI), and the reaction is exothermic. MOS-CuNPs also removed various cationic and anionic dyes from the solution. Other than RhB dye, MOS-CuNPs could remove other dyes studied without a reducing agent. The mechanism of removal of pollutants (Cr and dyes) might be due to electrostatic interaction and reduction process. Further, MOS-CuNPs showed antimicrobial effects against bacteria and fungi.

Declaration of competing interest

The authors declare that they have no known competing financial interests or personal relationships that could have appeared to influence the work reported in this paper.

Acknwoledgment

The author extends her appreciation to the deputyship for Research & Innovation, Ministry of Education in Saudi Arabia for funding this research work through the project number (IF2/PSAU/2022/01/23213.

Appendix A. Supplementary material

Supplementary data to this article can be found online at https://doi.org/10.1016/j.sjbs.2023.103820.

References

Adebayo, I.A., Arsad, H., Samian, M.R., 2018. Total phenolics, total flavonoids, antioxidant capacities, and volatile compounds gas chromatography-mass spectrometry profiling of *Moringa oleifera* ripe seed polar fractions. Pharmacogn. Mag. 14, 191.

Adesina, O.A., Taiwo, A.E., Akindele, O., Igbafe, A., 2021. Process parametric studies for decolouration of dye from local 'tie and dye'industrial effluent using *Moringa oleifera* seed. S. Afr. J. Chem. Eng. 37, 23–30.

Ahmed, I.A., Hussein, H.S., Ragab, A.H., AlMasoud, N., Ghfar, A.A., 2021. Investigation the effects of green-synthesized copper nanoparticles on the performance of activated carbon-chitosan-alginate for the removal of Cr (VI) from aqueous solution. Molecules 26, 2617.

Ahmed, M., Mavukkandy, M.O., Giwa, A., Elektorowicz, M., Katsou, E., Khelifi, O., Naddeo, V., Hasan, S.W., 2022. Recent developments in hazardous pollutants removal from wastewater and water reuse within a circular economy. npj Clean Water 5, 12.

Al-Enazi, N.M., Alsamhary, K., Ameen, F., 2023. Evaluation of citrus pectin capped copper sulfide nanoparticles against candidiasis causing candida biofilms. Environ. Res. 225, 115599.

Alhalili, Z., 2022. Green synthesis of copper oxide nanoparticles CuO NPs from Eucalyptus Globoulus leaf extract: adsorption and design of experiments. Arab. J. Chem. 15, 103739.

Al-Sou'od, K., 2012. Adsorption isotherm studies of chromium (VI) from aqueous solutions using jordanian pottery materials. APCBEE Proc. 1, 116–125.

Al-Tohamy, R., Ali, S.S., Li, F., Okasha, K.M., Mahmoud, Y.A.G., Elsamahy, T., Jiao, H., Fu, Y., Sun, J., 2022. A critical review on the treatment of dye-containing wastewater: ecotoxicological and health concerns of textile dyes and possible remediation approaches for environmental safety. Ecotoxicol. Environ. Saf. 231, 113160.

Amin, F., Khattak, B., Alotaibi, A., Qasim, M., Ahmad, I., Ullah, R., Bourhia, M., Gul, A., Zahoor, S., Ahmad, R., 2021. Green synthesis of copper oxide nanoparticles using *Aerva javanica* leaf extract and their characterization and investigation of in vitro antimicrobial potential and cytotoxic activities. Evidence-Based Complementary Alternative Med.

Ayub, A., Raza, Z.A., Majeed, M.I., Tariq, M.R., Irfan, A., 2020. Development of sustainable magnetic chitosan biosorbent beads for kinetic remediation of arsenic contaminated water. Int. J. Biol. Macromol. 163, 603–617.

Din, M.I., Arshad, F., Hussain, Z., Mukhtar, M., 2017. Green adeptness in the synthesis and stabilization of copper nanoparticles: catalytic, antibacterial, cytotoxicity, and antioxidant activities. Nanoscale Res. Lett. 12, 1–15.

Elango, M., Deepa, M., Subramanian, R., Mohamed Musthafa, A., 2018. Synthesis, characterization, and antibacterial activity of polyindole/Ag–Cuo nanocomposites by reflux condensation method. Polym.-Plast. Technol. Eng. 57, 1440–1451.

Flores, B., Ramírez, E., Moncada, A., Salinas, N., Fischer, R., Hernández, C., Mora-Sánchez, B., Sheleby-Elías, J., Jirón, W., Balcázar, J.L., 2022. Antimicrobial effect of *Moringa oleifera* seed powder against vibrio cholerae isolated from the rearing water of shrimp (*Penaeus vannamei*) postlarvae. Lett. Appl. Microbiol. 74, 238–246.

Geng, B., Jin, Z., Li, T., Qi, X., 2009. Kinetics of hexavalent chromium removal from water by chitosan-Fe0 nanoparticles. Chemosphere 75, 825–830.

Ghaffar, A., Kiran, S., Rafique, M.A., Iqbal, S., Nosheen, S., Hou, Y., Afzal, G., Bashir, M., Aimun, U., Yumei, H., 2021. Citrus paradisi fruit peel extract mediated green synthesis of copper nanoparticles for remediation of disperse yellow 125 dye. Desalin. Water Treat. 212, 368–375.

Ghebremichael, K., Gebremedhin, N., Amy, G., 2010. Performance of *Moringa oliefera* as a biosorbent for chromium removal. Water Sci. Technol. 62, 1106–1111.

Goswami, A., Raul, P.K., Purkait, M.K., 2012. Arsenic adsorption using copper (II) oxide nanoparticles. Chem. Eng. Res. Des. 90, 1387–1396.

Gurunathan, S., Han, J.W., Dayem, A.A., Eppakayala, V., Kim, J.-H., 2012. Oxidative stress-mediated antibacterial activity of graphene oxide and reduced graphene oxide in *Pseudomonas aeruginosa*. Int. J. Nanomed., 5901–5914

Ismail, M., Gul, S., Khan, M.I., Khan, M.A., Asiri, A.M., Khan, S.B., 2019. Green synthesis of zerovalent copper nanoparticles for efficient reduction of toxic azo dyes congo red and methyl orange. Green Process. Synth, 8, 135–143.

Jia, L., Zhou, W., Huang, X., Zhang, Y., Zhang, Q., Tan, X., Yu, T., 2019. Enhanced adsorption of Cr (VI) on biobr under alkaline conditions: interlayer anion exchange. Environ. Sci. Nano 6, 3601–3610.

Katata-Seru, L., Moremedi, T., Aremu, O.S., Bahadur, I., 2018. Green synthesis of iron nanoparticles using Moringa oleifera extracts and their applications: removal of nitrate from water and antibacterial activity against *Escherichia coli*. J. Mol. Liq. 256, 296–304.

Katsayal, B.S., Sallau, A.B., Muhammad, A., 2022. Kinetics and thermodynamics of Cr (VI) reduction by *Tamarindus indica* methanol leaves extract under optimized reaction conditions. Beni-Suef Univ. J. Basic Appl. Sci. 11, 1–10.

Khamis Soliman, N., Moustafa, A.F., Aboud, A.A., Halim, K.S.A., 2019. Effective utilization of Moringa seeds waste as a new green environmental adsorbent for removal of industrial toxic dyes. J. Mater. Res. Technol. 8, 1798–1808.

Khani, R., Roostaei, B., Bagherzade, G., Moudi, M., 2018. Green synthesis of copper nanoparticles by fruit extract of Ziziphus *spina-christi* (l.) willd.: application for adsorption of triphenylmethane dye and antibacterial assay. J. Mol. Liq. 255, 541–549.

Lopes, T.D.P., da Costa, H.P.S., Pereira, M.L., da Silva Neto, J.X., de Paula, P.C., Brilhante, R.S.N., Oliveira, J.T.A., Vasconcelos, I.M., Sousa, D.O.B., 2020. Mo-cbp4, a purified chitin-binding protein from *Moringa oleifera* seeds, is a potent antidermatophytic protein: *in vitro* mechanisms of action, *in vivo* effect against infection, and clinical application as a hydrogel for skin infection. Int. J. Biol. Macromol. 149, 432–442.

Ma, X., Zhou, S., Xu, X., Du, Q., 2022. Copper-containing nanoparticles: mechanism of antimicrobial effect and application in dentistry-a narrative review. Front. Surg. 9.

Mahmoud, A.E.D., Al-Qahtani, K.M., Alflaij, S.O., Al-Qahtani, S.F., Alsamhan, F.A., 2021. Green copper oxide nanoparticles for lead, nickel, and cadmium removal from contaminated water. Sci. Rep. 11, 12547.

Mohammadi, P., Heravi, M.M., Sadjadi, S., 2020. Green synthesis of Ag NPs on magnetic polyallylamine decorated g-C_3N_4 by *Heracleum persicum* extract: efficient catalyst for reduction of dyes. Sci. Rep. 10, 6579.

Mohan, S., Singh, Y., Verma, D.K., Hasan, S.H., 2015. Synthesis of cuo nanoparticles through green route using citrus limon juice and its application as nanosorbent forCr (VI) remediation: process optimization with RSM and ANN-GA based model. Process Saf. Environ. Prot. 96, 156–166.

Naikoo, G., Al-Mashali, F., Arshad, F., Al-Maashani, N., Hassan, I.U., Al-Baraami, Z., Faruck, L.H., Qurashi, A., Ahmed, W., Asiri, A.M., 2021. An overview of copper nanoparticles: synthesis, characterisation and anticancer activity. Curr. Pharm. Des. 27, 4416–4432.

Noli, F., Dafnomili, A., Dendrinou-Samara, C., Kapnisti, M., Pavlidou, E., 2023. Critical parameters and mechanisms of chromium removal from water by copper-based nanoparticles. Water Air Soil Pollut. 234, 12.

Nouhi, S., Kwaambwa, H.M., Gutfreund, P., Rennie, A.R., 2019. Comparative study of flocculation and adsorption behaviour of water treatment proteins from *Moringa peregrina* and *Moringa oleifera* seeds. Sci. Rep. 9, 17945.

Nova, E., Redondo-Useros, N., Martínez-García, R.M., Gómez-Martínez, S., Díaz-Prieto, L.E., Marcos, A., 2020. Potential of *Moringa oleifera* to improve glucose control for the prevention of diabetes and related metabolic alterations: a systematic review of animal and human studies. Nutrients 12, 2050.

Padmavathi, A.R., Das, A., Priya, A., Sushmitha, T.J., Pandian, S.K., Toleti, S.R., 2020. Impediment to growth and yeast-to-hyphae transition in *Candida Albicans* by copper oxide nanoparticles. Biofouling 36, 56–72.

Raffi, M., Mehrwan, S., Bhatti, T.M., Akhter, J.I., Hameed, A., Yawar, W., 2010. Investigations into the antibacterial behavior of copper nanoparticles against *Escherichia coli*. Ann. Microbiol. 60, 75–80.

Rafique, M.A., Jamal, A., Ali, Z., Kiran, S., Iqbal, S., Nosheen, S., Ansar, Z., Hossain, M.B., 2022. Biologically synthesized copper nanoparticles show considerable degradation of reactive red 81 dye: an eco-friendly sustainable approach. BioMed Res. Int.

Ragadhita, R., Nandiyanto, A.B.D., 2021. How to calculate adsorption isotherms of particles using two-parameter monolayer adsorption models and equations. Indonesian J. Sci. Technol. 6, 205–234.

Rivero-Huguet, M., Marshall, W.D., 2009. Reduction of hexavalent chromium mediated by micro-and nano-sized mixed metallic particles. J. Hazard. Mater. 169, 1081–1087.

Singaravelu, D.K., Binjawhar, D.N., Ameen, F., Veerappan, A., 2022. Lectin-fortified cationic copper sulfide nanoparticles gain dual targeting capabilities to treat carbapenem-resistant *Acinetobacter baumannii* infection. ACS Omega 7, 43934–43944.

Singh, P.K., Kumar, P., Hussain, M., Das, A.K., Nayak, G.C., 2016. Synthesis and characterization of cuo nanoparticles using strong base electrolyte through electrochemical discharge process. Bull. Mater. Sci. 39, 469–478.

Tahir, A., Quispe, C., Herrera-Bravo, J., Iqbal, H., Anum, F., Javed, Z., Sehar, A., Sharifi-Rad, J., 2022. Green synthesis, characterization and antibacterial, antifungal, larvicidal and anti-termite activities of copper nanoparticles derived from *Grewia asiatica* L. Bull. Natl. Res. Centre. 46, 1–11.

Tumolo, M., Ancona, V., De Paola, D., Losacco, D., Campanale, C., Massarelli, C., Uricchio, V.F., 2020. Chromium pollution in european water, sources, health risk, and remediation strategies: an overview. Int. J. Environ. Res. Public Health 17, 5438.

Wang, L., Hu, C., Shao, L., 2017. The antimicrobial activity of nanoparticles: present situation and prospects for the future. Int. J. Nanomed. 12, 1227.

Ye, J., Wang, Y., Xu, Q., Wu, H., Tong, J., Shi, J., 2021. Removal of hexavalent chromium from wastewater by Cu/Fe bimetallic nanoparticles. Sci. Rep. 11, 10848.

Zhitkovich, A., 2011. Chromium in drinking water: sources, metabolism, and cancer risks. Chem. Res. Toxicol. 24, 1617–1629.